European Journal of Mechanics / A Solids 100 (2023) 104988

Contents lists available at ScienceDirect

European Journal of Mechanics / A Solids

journal homepage: www.elsevier.com/locate/ejmsol

A comprehensive study for the effect of sample geometry and lateral pressure on shear fractures using the short core in compression (SCC) method

Mahmoud Alneasan[a], Abdel Kareem Alzo'ubi[b,*], Nader Okasha[b]

[a] Civil Engineering Department, Tishreen University. Latakia, Syria
[b] Civil Engineering Department, Abu Dhabi University. Al Ain, United Arab Emirates

ARTICLE INFO

Keywords:
Short core in compression (SCC)
Shear fractures
Stress intensity factor
Lateral pressure
Fracture toughens
Fracture path

ABSTRACT

Shear fractures are common in the rock mass, especially with increasing depth, due to the increase in lateral pressure. Hence, investigating these fractures is crucial for improving the stability and safety of underground structures at greater depths. The Short Core in Compression (SCC) method has recently been used by some researchers to generate shear fractures under mode II loading and initiation due to the ease of sample preparation and lateral pressure application. This study examines the impact of sample geometry and lateral pressure on the formation of shear fractures in rocks, by conducting numerical and experimental investigations on SCC samples. In this paper, the effect of sample shape, notch length, and lateral pressure was evaluated depending on the shear and the maximum principal stress distribution. To the best knowledge of the authors, the impact of these factors has not been sufficiently explored in the literature. Moreover, the mode II stress intensity factor, fracture toughness, and fracture path were investigated. The results provided the stress intensity factor for different geometries of the SCC sample that can be used for many applications in mechanical and geological engineering. Our findings showed that the resulting fracture must be evaluated due to the possibility of crack growth under shear σ_{xy} or maximum principal stress σ_{max}, especially for Notch Length/Diameter $\geq$0.5. Additionally, lateral pressure mainly affects the distribution and magnitude of σ_{max}, such that σ_{max} is inversely proportional to this pressure. The results showed that the SCC sample with Height/Diameter = 2 is preferred because σ_{max} is minimum for this sample shape, which promoted fracture growth under shear stress not tensile stress. Furthermore, as the lateral pressure increases, mode II fracture toughness significantly increases and the number of fragments that spalled off the specimen along the fracture path decreases.

1. Introduction

The study of fractures in rock mass, concrete, and other brittle materials has wide scientific and practical applications in various fields of civil engineering, rock mechanics, geological engineering, material science, and fracture mechanics (Alneasan and Behnia, 2022b; Alneasan et al., 2020; Bahrami et al., 2022; Zhang et al., 2022b). Shear fractures are a common occurrence in the deep underground crust due to the effect of high in-situ stresses. Analyzing these fractures is critical to understand the mechanism of growth of these fractures under the influence of different loading patterns, and thus increase the safety and stability of mines, underground infrastructures, buildings, etc. (Alzo'ubi, 2014; Guo et al., 2020; Kim and Larson, 2021; Li et al., 2020; Szwedzicki, 2003).

Most research on this topic focused on mode I fractures that grow under tension. Various methods and sample geometries such as Semi-Circular Specimens (SCB) (Ayatollahi et al., 2006; Kuruppu et al., 2014), Cracked Chevron Notched Brazilian Disc (CCNBD) (Fowell et al., 1995), Edge Cracked Short Bend Beam (ECSBB) (Aliha and Ayatollahi, 2010; Mousavi et al., 2020), and Chevron Bending (CB) (Franklin et al., 1988) were suggested to study these fractures. Studies related to mode II (shear) fractures are fewer than those relate to pure mode I fractures. This is because measuring fracture parameters such as fracture toughness under pure shear loads is more difficult than that under pure tension (Wang et al., 2011). The issue becomes more complicated when studying shear fractures under both mode II loading and mode II initiation. This is because the geometry of the sample and the applied loads

* Corresponding author.
E-mail addresses: mahmoud.alneasan@tishreen.edu.sy (M. Alneasan), abdel.alzoubi@adu.ac.ae (A.K. Alzo'ubi), nader.okasha@adu.ac.ae (N. Okasha).

https://doi.org/10.1016/j.euromechsol.2023.104988
Received 8 October 2022; Received in revised form 15 February 2023; Accepted 29 March 2023
Available online 30 March 2023

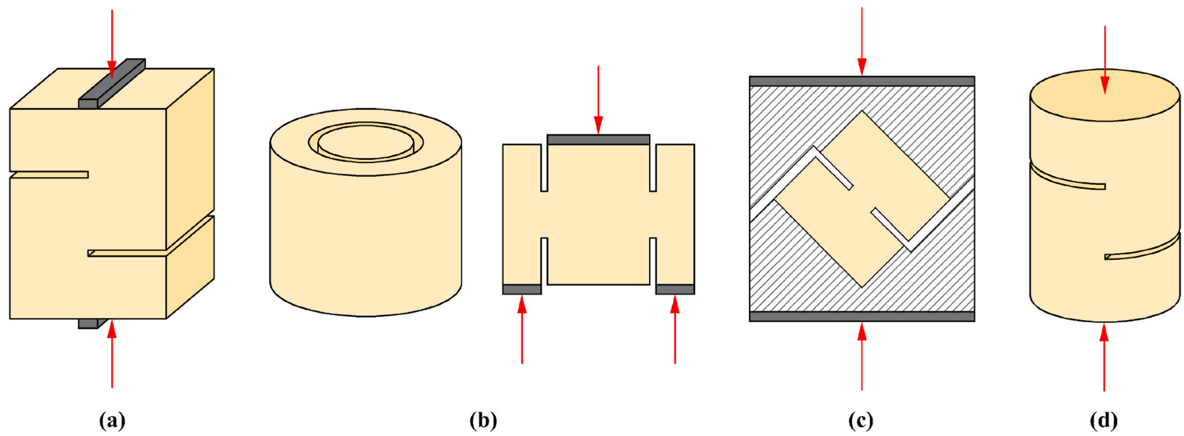

Fig. 1. Different suggested methods for studying shear fractures under both the mode II loading and the mode II initiation, (a) SBC, (b) PTS, (c) SBT, and (d) SCC.

must ensure that crack growth initiates under shear stress ($\sigma_{r\theta}$), not under tensile stress ($\sigma_{\theta\theta}$). Some methods were suggested to tackle this problem, see Fig. 1. These methods include Short Beam in Compression (SBC) (Watkins and Liu, 1985), Punch Through Shear (PTS) (Backers and Stephansson, 2012), Shear Boxing Test (SBT) (Rao et al., 2003) and Short Core in Compression (SCC) (Jung et al., 2016), as shown in Fig. 1-a, b, c, and d, respectively. The first three specimens in Fig. 1 are difficult to prepare and to be notched in comparison with the SCC specimen. It is worth mentioning that, the SCC specimen can be easily prepared by extracting a core with diameter D from a rock block and then cutting two parallel horizontal notches into the specimen. As a result, the use of the SCC configuration is prevalent among researchers investigating shear fracture initiation and development. Furthermore, the SCC sample is the optimal choice for applying lateral pressure, which is one of the central focuses of this study.

Several researchers have studied and developed the SCC method to investigate shear fractures in rocks. Jung et al. (2016) suggested the SCC method with H/D = 2 to generate shear fractures under the mode II loading and initiation, where H and D are the height and diameter of the SCC sample, respectively. Xu et al. (2020) evaluated the SCC method to measure mode II fracture toughness by comparing its results with those of the SCB method. Yao et al. (2021) used SCC samples with H/D = 1 in marble to investigate dynamic mode II fracture toughness under hydrostatic pressure. In addition, the effect of thermal treatment on the dynamic mode II fracture toughness of granite was investigated by Li et al. (2022b) by using SCC samples with H/D = 1. Li et al. (2022a); Zhang et al. (2023) investigated the dynamic shear behavior of SCC samples using the digital image correlation technique and found that the new shear fracture initiates from tips of two notches and the fracture path is nearly independent of the loading rate. Yao et al. (2022) utilized SCC and PTS samples to investigate dynamic mode II fracture toughness of marble under various in situ loading conditions, they provided empirical equations for the effect of the loading rate, confining pressure, and sample geometry on the fracture toughness. Zhang et al. (2022a) studied the effect of confining pressure on shear fractures induced in SCC samples of granite and concluded that the peak load, shear modulus, nominal shear strength and mode II fracture toughness of SCC specimens increase approximatively linearly with confining pressure. Taking into account previous studies, the SCC method still needs further investigation to study important factors related to the distribution of stresses in SCC samples, and to predict mode II stress intensity factors and fracture toughness in different geometries of SCC samples, especially when lateral pressure is considered. Therefore, a numerical code based on the Displacement Discontinuity Method (DDM) was extended in this study to investigate the effect of sample geometry such as sample shape, notch length, and lateral pressure on the growth of shear fractures in SCC samples. The effect of sample geometry and lateral pressure were evaluated depending on distribution of shear and maximum principal stress, and depending on the mode II stress intensity factor and fracture toughness. Furthermore, experimental tests were conducted on 12 SCC samples under four values of lateral pressure to study the effect of confinement on mode II fracture toughness and fracture path.

2. Preparation of SCC specimen

As shown in Fig. 2-a, the SCC sample is cylindrical and has two

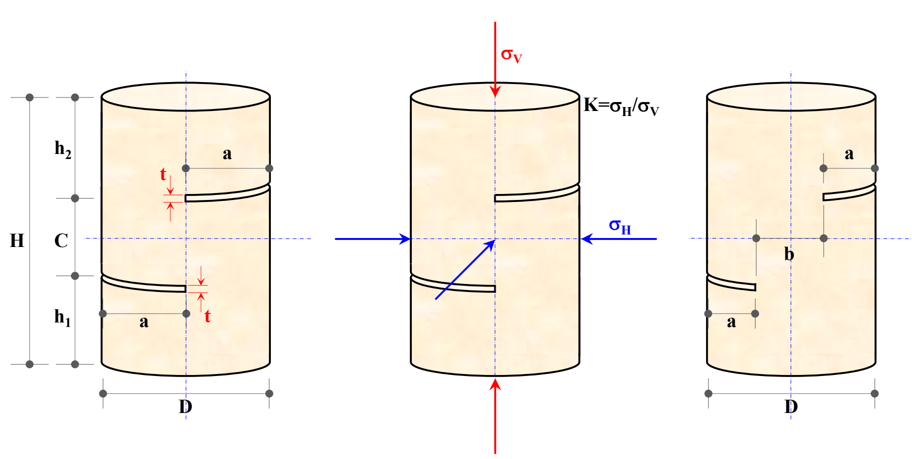

Fig. 2. (a) Geometry of the SCC sample, (b) SCC sample under lateral pressure, (c) SCC sample with different notches lengths.

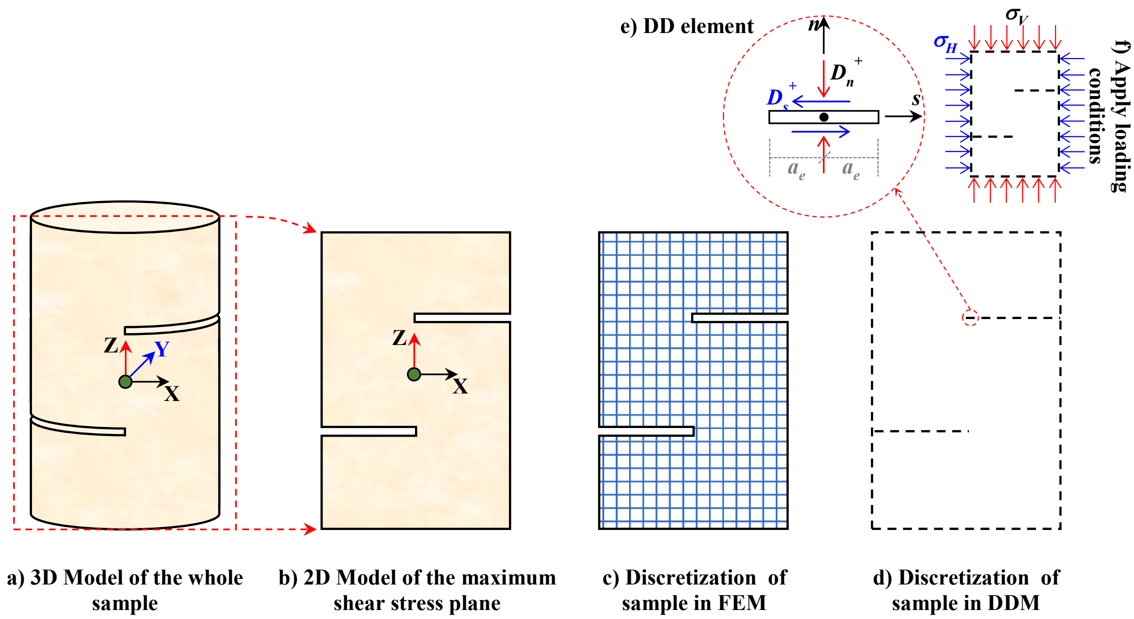

Fig. 3. Modeling of SCC sample depending on FEM and DDM.

parallel notches. Different values of the H/D ratio can be selected to prepare SCC samples. Therefore, the effect of sample shape was numerically investigated in this work by choosing different values of H/D ratio from 0.5 to 2. The vertical distance between the tips of the two notches is C, and the ratio of C/H has a great effect on the magnitude and distribution of shear stress along the bridge between the tips of the two notches. The effect of the C/H ratio on the shear and maximum principal stress fields, and mode II stress intensity factor K_{II} was numerically investigated by Xu et al. (2020) for H/D = 2, and they showed that by increasing the C/H ratio, shear and maximum principal stress along the bridge between notches tips decreases. In this paper, we investigate the effect of sample configuration and lateral pressure on the factors that influence the propagation of shear cracks between the tips of two notches. These factors are the stress fields and the mode II stress intensity factor. The effects of H/D, a/D, and K ratios on the phenomenon of shear fractures in SCC samples were considered. Where K is the ratio of lateral to vertical stresses under conventional triaxial conditions (Fig. 2-b). Therefore, this study examines the impact of the following factors on the onset and propagation of shear fractures in SCC samples: 1) the effect of sample shape, by choosing different values of the H/D ratio between 0.5 and 2, 2) the effect of lateral pressure for K values between 0.0 (uniaxial case) and 1 (hydrostatic case), 3) the effect of notch length, a, and the horizontal distance between tips of two notches, b, by controlling of a/D ratio within values between 0.45 and 0.55.

3. Numerical procedure

Mode II shear fractures using the short core in compression (SCC) method were modeled firstly by Jung et al. (2016) using the Finite Element Method (FEM) and considering the SCC approach. Some researchers developed similar FEM models but considered other dimensions of the SCC sample (Xu et al., 2020) and lateral pressure (Yao et al., 2021). Numerical modeling using the FEM requires dividing the entire area or volume into finite elements, and each element contains at least three or four nodes (Alzo'ubi, 2016). So in FEM, the number of resulting equations is large and numerical modeling requires a considerable computational time. Additionally, any modification to the model dimensions requires a geometric reconstruction of the sample. Therefore, the DDM, which is a branch of the Boundary Element Method (BEM) was used in this work to model the SCC specimens. In the DDM, only the boundary and discontinuities of interest, such as the horizontal notches, are discretized into N Displacement Discontinuity (DD) elements (Crouch et al., 1983). Therefore, the number of resulting equations decreases, and the model is solved in lesser time than the FEM.

The basic model is a 3D model (Fig. 3-a), however, Yao et al. (2021) argued that due to the symmetric configuration of the SCC sample, the XZ plane in the middle of the SCC sample that contains two parallel notches represents the plane of maximum shear stress along the failure surface (Fig. 3-b). Therefore, this plane is the critical plane for shear fracture and can be modeled in a 2D manner to represent the stress distribution and state when a shear failure occurs in the SCC sample. Fig. 3-c shows how the whole region of the SSC sample is discretized depending on the FEM, while Fig. 3-d shows how the boundary of the SCC sample with two horizontal notches is discretized into DD elements.

A DD element (Fig. 3-e) has one node at its center and it is subjected to normal stress, σ_n, and shear stress, σ_s, or normal displacement, u_n, and shear displacement, u_s, or stress and displacement simultaneously. This depends on the boundary conditions. For the current study, two types of boundary conditions were adopted to simulate the SCC sample under uniaxial and lateral stress states (conventional triaxial conditions). Firstly, under the uniaxial stress state, only the upper and lower surfaces of the SCC sample are subjected to vertical stress σ_V, so the DD elements of these surfaces are modeled as$\sigma_n = \sigma_V$, $\sigma_s = 0.0$, $u_s = u_n =$ free, while other DD elements for the side surfaces and inner notches are modeled as free traction elements ($\sigma_n = \sigma_s = u_s = u_n =$ free). Secondly, in the lateral stress state, the upper and lower surfaces are subjected to vertical stress σ_V and the side surfaces are subjected to lateral stress σ_H, so the DD elements for the upper and lower surfaces are modeled as $\sigma_n = \sigma_V$, $\sigma_s = 0.0$, $u_s = u_n =$ free, while DD elements for the side surfaces are modeled as $\sigma_n = \sigma_H$, $\sigma_s = 0.0$, $u_s = u_n =$ free, other DD elements for inner notches are modeled as free traction elements. The displacement discontinuities vector (D_n, D_s) correlates to the boundary conditions vector (B_n, B_s) via the influence coefficients matrix (A). Where D_n and D_s are normal and shear displacement discontinuities at the center of the DD element, respectively. B_n and B_s are normal and shear displacement of stress that applied to the DD element. Finally, displacement discontinuities are determined by solving a system of algebraic equations ($B = A \times D$). As shown in Fig. 3-e, positive D_n means that element surfaces approach each other and the element is under compression, while positive D_s means that the upper surface moves to the left relative to the lower

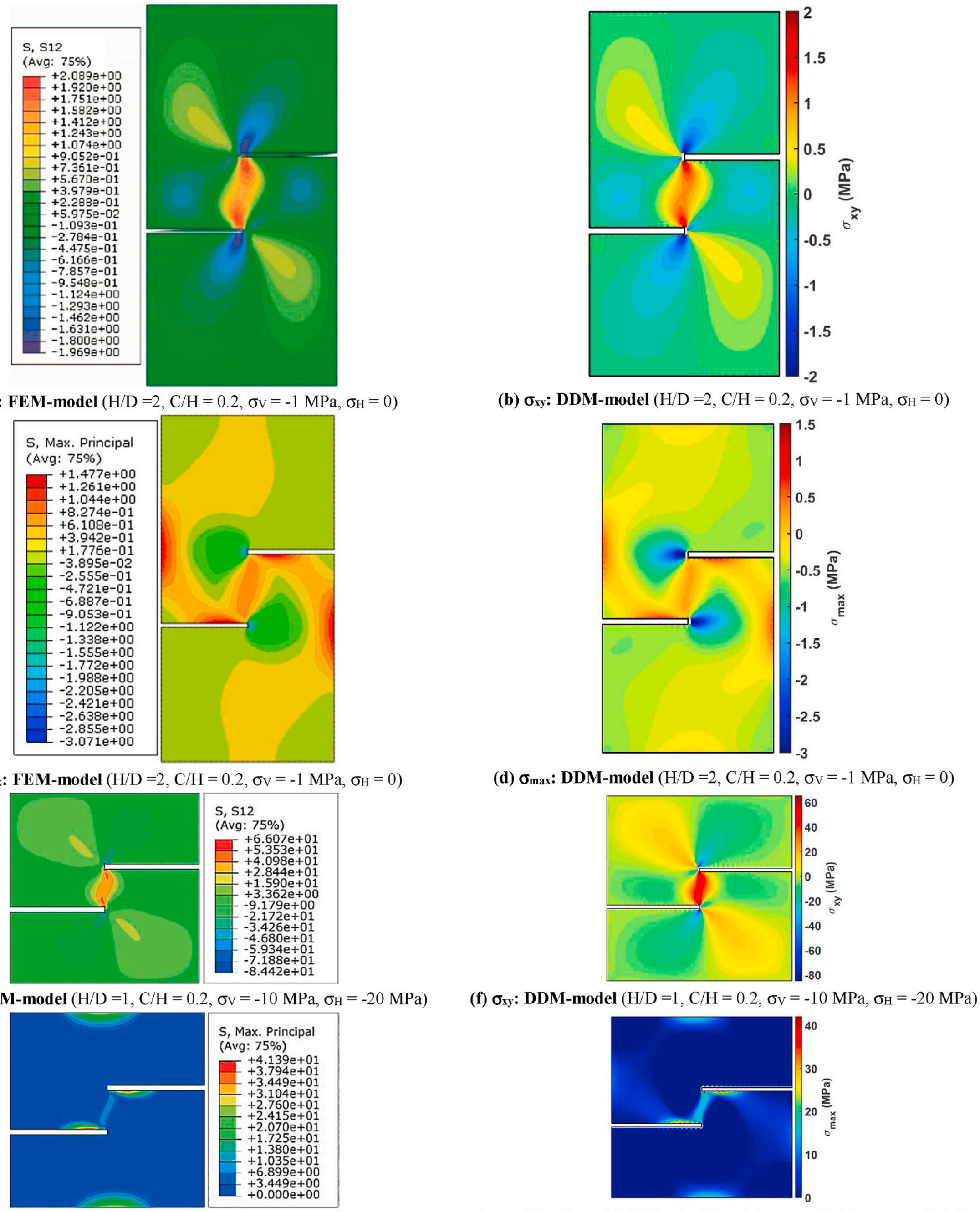

(a) σ_{xy}: FEM-model (H/D =2, C/H = 0.2, σ_V = -1 MPa, σ_H = 0)

(b) σ_{xy}: DDM-model (H/D =2, C/H = 0.2, σ_V = -1 MPa, σ_H = 0)

(c) σ_{max}: FEM-model (H/D =2, C/H = 0.2, σ_V = -1 MPa, σ_H = 0)

(d) σ_{max}: DDM-model (H/D =2, C/H = 0.2, σ_V = -1 MPa, σ_H = 0)

(e) σ_{xy}: FEM-model (H/D =1, C/H = 0.2, σ_V = -10 MPa, σ_H = -20 MPa)

(f) σ_{xy}: DDM-model (H/D =1, C/H = 0.2, σ_V = -10 MPa, σ_H = -20 MPa)

(g) σ_{max}: FEM-model (H/D =1, C/H = 0.2, σ_V = -10 MPa, σ_H = -20 MPa)

(h) σ_{max}: DDM-model (H/D =1, C/H = 0.2, σ_V = -10 MPa, σ_H = -20 MPa)

Fig. 4. Verification of the extended TDCPC, stage 1: prediction of shear and maximum principal stresses, (a and c) by Xu, Yao [2], (e and g) by Yao, Xu [3], (b, d, f, and h) DDM code of the current study.

surface indicating left-lateral slip.

A two-dimensional crack propagation code (TDCPC) based on the DDM method was developed previously by Alneasan and Behnia (2022a) to solve different problems in rock mechanics (Alneasan et al., 2022a, 2022b). In this work, this code was extended to model SCC samples under uniaxial and biaxial compressive stress states (Fig. 3-f). As shown in the next section, the extended code was verified by comparing its result with similar studies in fracture mechanics. For the developed numerical code, two cases should be distinguished when predicting stress fields and calculating stress intensity factors and fracture toughness. The first case is the uniaxial stress state where the upper and lower surfaces of the SCC sample are only subjected to increasing vertical pressure $\sigma_1 = \sigma_V$ until the onset of fracture, and the side surfaces and internal notches are pressure-free. The second case is the lateral stress state that corresponds to the conventional triaxial test ($\sigma_1 = \sigma_V$ and $\sigma_2 = \sigma_3 = \sigma_H \neq 0$), in this case, the upper and lower surfaces of the SCC sample are subjected to increasing vertical stress $\sigma_1 = \sigma_V$, and the side surfaces are subjected to constant pressure $\sigma_2 = \sigma_3 = \sigma_H$ until the onset of fracture. In this study there a rubber membrane was used to surround the SCC sample during the conventional triaxial test by using Hoek cell. This membrane does not allow the hydraulic oil to enter the two tiny notches, so the notches surfaces are not directly subjected to the hydraulic pressure as in the experiments conducted by Zhang et al. (2022a). Thus, there is no need to numerically simulate the SCC sample by considering the effect of hydraulic pressure inside the two notches.

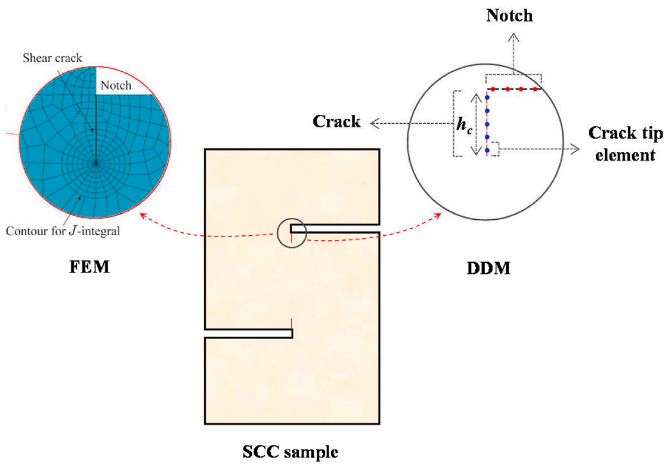

Fig. 5. SCC specimen with secondary shear cracks modeled by FEM as well as DDM.

3.1. Verification of the extended TDCPC

The extended TDCPC based on the DDM model was verified by comparing its results with the numerical results of previous studies for two geometries of the SCC sample. In the first geometry, the H/D ratio is 2, and the SCC sample was modeled by Xu et al. (2020) using the FEM in a 3D manner. In the second geometry, the H/D ratio is 1, and the SCC sample was modeled by Yao et al. (2021) using the FEM in a 3D and 2D manner.

In the first stage, shear and maximum principal stress fields were determined and compared with that of previous similar studies. Fig. 4-a and Fig. 4-b shows shear stress σ_{xy} and maximum principal stress σ_{max} predicted by Xu, Yao [2] using the FEM model for H/D = 2, C/H = 0.2, $\sigma_V = -1$ MPa and $\sigma_H = 0$ (uniaxial stress case). σ_{xy} and σ_{max} were predicted in this work under the same mentioned conditions by using the extended DDM code and they are shown in Fig. 4-b and Fig. 4-d, respectively. Comparing Fig. 4-a and Fig. 4-b, it can be noted that σ_{xy} predicted by the DDM model has the same distribution and values as predicted by the FEM model. Under uniaxial stress case ($\sigma_V = -1$ and $\sigma_H = 0$ MPa), σ_{xy} changes between −2 and +2 MPa over the entire SCC sample, and it has the maximum value at the notch tip. The same can be noted for σ_{max} by comparing Fig. 4-d and Fig. 4-c σ_{max} predicted by the DDM model has the same distribution and magnitude as that predicted by the FEM model. In addition, to ensure the validity of the extended DDM model under biaxial stress state and for other SCC geometry (H/D = 1), σ_{xy} and σ_{max} were predicted by the DDM model under H/D = 1, C/H = 0.2, $\sigma_V = -10$ MPa, $\sigma_H = -20$ MPa, and compared with that predicted by Yao, Xu [3] using the FEM model under the same mentioned conditions. Comparing Fig. 4-e and Fig. 4-f for σ_{xy}, Fig. 4-g and Fig. 4-h for σ_{max}, it can be noted that σ_{xy} and σ_{max} predicted by the DDM model agree with that predicted by the FEM model under the effect of lateral stress $\sigma_H = -20$ MPa.

In the second stage of verification of the extended TDCPC, the mode II stress intensity factor (K_{II}) was calculated using the extended TDCPC code for the previous two geometries (H/D = 2 and 1) and compared with those found in similar studies. Yao et al. (2021) pointed out that the maximum shear stress concentrates along the vertical bridge between two notch tips and it is maximized at these tips, the fracture initiates at lower and upper notch tips, and secondary shear cracks are required to calculate K_{II}. Moreover, by using the digital image correlation technique on SCC samples of granite, Zhang et al. (2023) found that new cracks first initiate from two notch tips and then propagate toward the central area in the expected shear fracture band. To apply the traditional fracture mechanics theory to the SCC specimen, the secondary shear crack is necessary for accurately determining the stress intensity factor in the fracture process, and the K_{IIC} can be further determined precisely when a crack tip exists along the shear bridge between tips of the two horizontal notches (Atkinson, 1987; Horii and Nemat-Nasser, 1985, 1986; Nemat-Nasser and Horii, 1982). Fig. 5 shows an SCC specimen with secondary shear cracks modeled by FEM as well as DDM. The length of the shear crack, h_c, is divided into N_c DD elements. Stress intensity factors in the study of Xu et al. (2020); Yao et al. (2021) were calculated using finite element analysis (FEA) with the J-integral method. In our work the K_{II} was computed for the crack tip using the DD analysis as shown by Shou and Crouch (1995) in Equation (1):

$$K_{II} = \frac{G}{4(1-\nu)}\sqrt{\frac{2\pi}{a_e}}D_s^{Tip} \tag{1}$$

where G and ν are shear modulus and Poisson's ratio, respectively. D_s^{Tip} is the shear displacement discontinuity at the crack tip element. a_e is half the length of the crack tip element. Fig. 6-a shows the change in K_{II} as a function of the C/H ratio for H/D = 2. This figure shows that the K_{II} determined by the extended TDCPC code is in good agreement with that of Xu et al. (2020) for different bridge lengths (different C/H ratios). Fig. 6-b shows K_{II} as a function of vertical stress σ_V under lateral pressure σ_H = 10 MPa, while Fig. 6-c shows the effect of vertical and lateral pressure on the K_{II}. These two figures show good agreement between our results and those of Yao et al. (2021). Accordingly, the extended TDCPC is valid to model SCC samples under uniaxial and lateral stress states.

4. Results and discussions

The numerical results constitute the main section of the results of this study, with a set of experimental results testing the effects of lateral pressure on SCC samples with a geometry of H/D = 2. For H/D = 1, the effect of lateral pressure was investigated by Yao et al. (2021). In this paper, the focus of the numerical and experimental results was on C/H = 0.15. This is to increase the effect of shear stress along the bridge

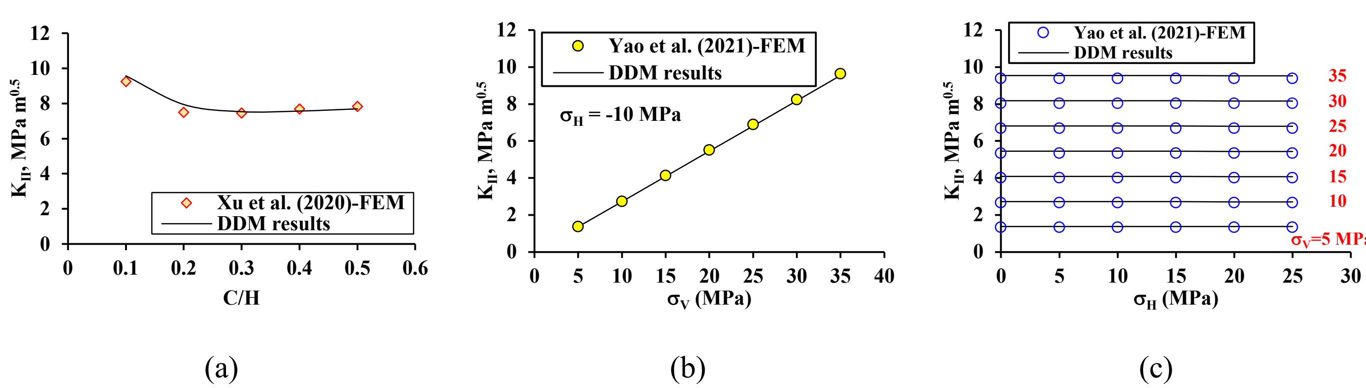

Fig. 6. Verification of the K_{II} with the results of (a) Xu et al. (2020) (H/D = 2) and (b, c) Yao et al. (2021) (H/D = 1).

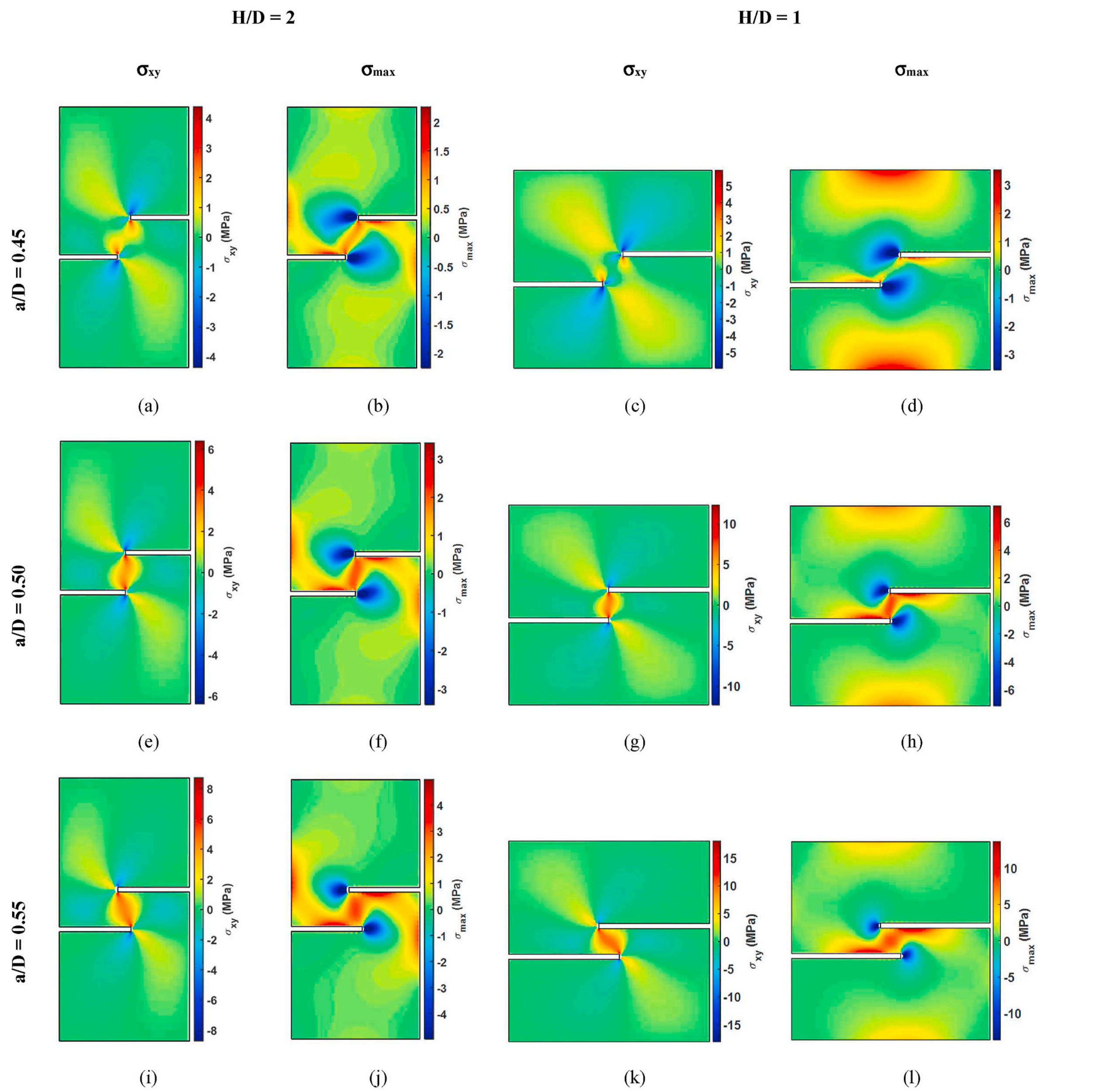

Fig. 7. The effect of a/D ratio on the shear and maximum principal stress fields in SCC samples for H/D = 2 and 1, d/H = 0.5, C/H = 0.15, K = 0.0, $\sigma_V = -1$ MPa.

between tips of two notches and to ensure the growth of shear fracture from the notch tip. As mentioned previously, the effect of the C/H ratio was investigated by Xu et al. (2020) for an SCC sample with a geometry of H/D = 2, where they concluded that the shear and maximum principal stresses increase with decreasing C/H ratio.

4.1. The effect of notch length (a/D ratio) on stress fields

The effect of notch length was investigated by choosing three values for the a/D ratio (0.45, 0.5, and 0.55). The effect of the a/D ratio on the shear and maximum principal stress fields in SCC samples for H/D = 2 and 1, determined by DDM is shown in Fig. 7. The case with a/D = 0.45, is called under-cut where the tips of two notches are horizontally spaced away from each other. Maximum shear stress between notches tips does not form a continuous bridge for two SCC geometries (H/D = 2 and 1, Fig. 7-a,c). For H/D = 2 (Fig. 7-b), the maximum principal stress is continuous between notches tips and it has a tensile effect ($\sigma_{max} > 0.0$). Therefore, a tensile fracture can occur under the effect of this stress. For H/D = 1 (Fig. 7-d), σ_{max} is concentrated at the upper and lower surfaces of the SCC sample and does not form a continuous bridge between notches tips.

The case with a/D = 0.5, is an ideal case, where the horizontal distance between notch tips is zero. i.e., vertically aligned. σ_{xy} and σ_{max} are concentrated along the bridge between the two notch tips for H/D = 2 and 1 (Fig. 7-e,f,g,h). Therefore, a fracture can occur under the effect of σ_{xy} or σ_{max}. According to stress distribution, if the resulting fracture is almost vertical and straight between two notches (as in σ_{xy} bridge in Fig. 7-e,g), it is an ideal shear fracture. But if it is inclined to the right with respect to the vertical axis of the SCC sample, as is the case in σ_{max} bridge between notch tips (Fig. 7-f,h), it is likely not considered a shear fracture.

The case with a/D = 0.55, is called over-cut where the notches are horizontally (parallel to the top edge of the sample) overlapping each other. Compared to the case of a/D = 0.45 that is shown in Fig. 7-a,c, σ_{xy} in Fig. 7-i,k is continuous along the bridge between notches tips for H/D = 2 and 1. Therefore, shear fractures can grow in this case. But the

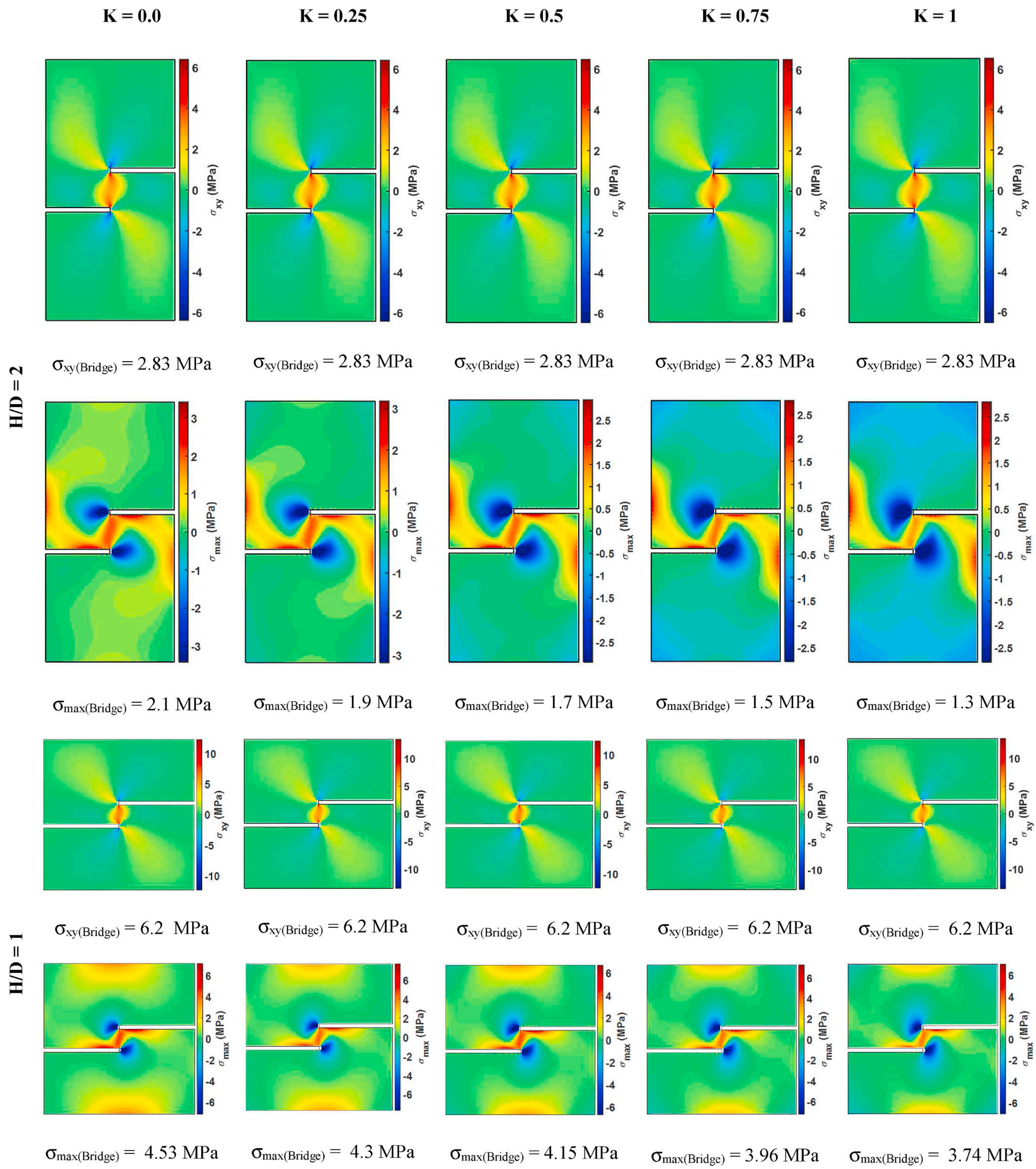

Fig. 8. The effect of lateral stress on σ_{xy} and σ_{max} for H/D = 2 and 1, d/H = 0.5, a/D = 0.5, C/H = 0.15, $\sigma_V = -1$ MPa.

resulting fracture must be evaluated to determine if it is caused by σ_{xy} or σ_{max}. When the fracture grows from notch tips tilted to the left with respect to the vertical axis of the SCC sample, as is the case of σ_{xy} bridge shown in Fig. 7-i,k, it is a shear fracture. But if the fracture grows tilted to the right with respect to the vertical axis of the sample, as is the case of σ_{max} bridge shown in Fig. 7-j,l, it is not considered a shear fracture, and it is likely to be a tensile fracture caused by σ_{max}.

Concerning the effect of the a/D ratio, it can be concluded that if a/D < 0.5 (under-cut case), it is not recommended to investigate shear fractures by SCC samples, especially for H/D = 1. For a/D = 0.5 and 0.55, the resulting fracture should be evaluated to determine whether this fracture is due to shear or maximum principal stress. Even in the ideal case (a/D = 0.5), the fracture can be caused by σ_{max}, not by σ_{xy}. Hence the importance of applying lateral pressure that reduces the effect

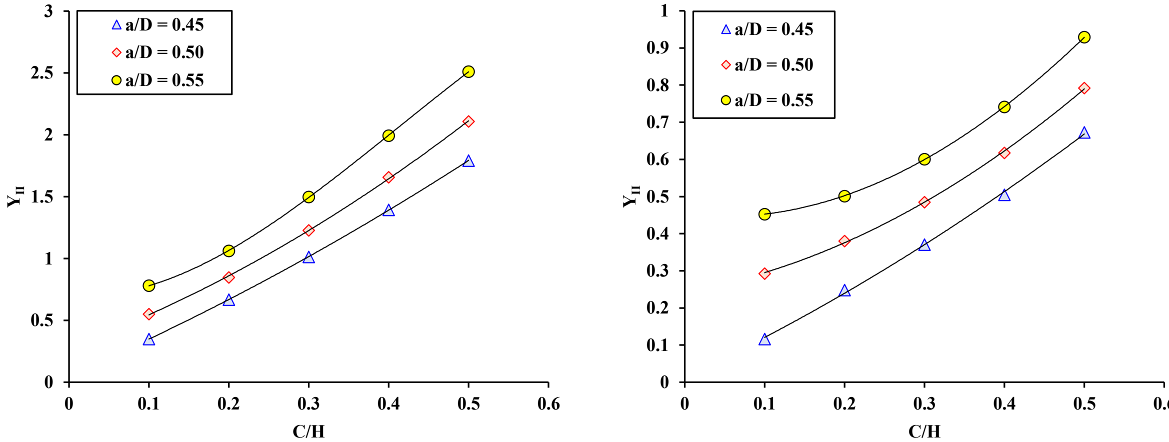

(a) H/D = 2 (b) H/D = 1

Fig. 9. The effect of the a/D ratio on Y_{II} for (a) H/D = 2 and (b) H/D = 1.

of σ_{max}, as shown in the following section.

4.2. *The effect of lateral stress (K ratio) on stress fields*

The effect of the lateral stress on σ_{xy} and σ_{max} for the ideal case (a/D = 0.5) is shown in Fig. 8. This figure shows that for H/D = 2 and 1, the distribution and magnitude of σ_{xy} are not affected by the lateral stress. For H/D = 2, the magnitude of the shear stress at the center of the bridge between notches tips ($\sigma_{xy(Bridge)}$) is 2.83 MPa for K from 0 to 1. The same point can be observed for H/D = 1, where $\sigma_{xy(Bridge)}$ is 6.2 MPa for all K ratios. The main effect of the lateral stress for two SCC geometries is on the magnitude of the σ_{max}. Fig. 8 shows that for H/D = 2, the magnitude of σ_{max} at the center of the bridge between notches tips ($\sigma_{max(Bridge)}$) decreases by about 38% when the K ratio increases from 0 to 1. For H/D = 1, $\sigma_{max(Bridge)}$ decreases by about 17% for K between zero and one. So the shape of the sample plays an important role in determining the effect of the lateral stress; σ_{max} in the SCC sample with the geometry of H/D = 2 is more affected by lateral stress than that of H/D = 1. This may give an advantage to the use of an SCC sample with H/D = 2 when the lateral stress is applied. This is because a significant decrease in $\sigma_{max(Bridge)}$ can be achieved by increasing the lateral stress, which inhibits the growth of tensile cracks caused by $\sigma_{max} > 0$ and promotes the growth of shear cracks caused by σ_{xy}.

4.3. *The effect of notch length (a/D ratio) and lateral stress on the stress intensity factor*

Mode II stress intensity factor K_{II} in the SCC sample can be computed

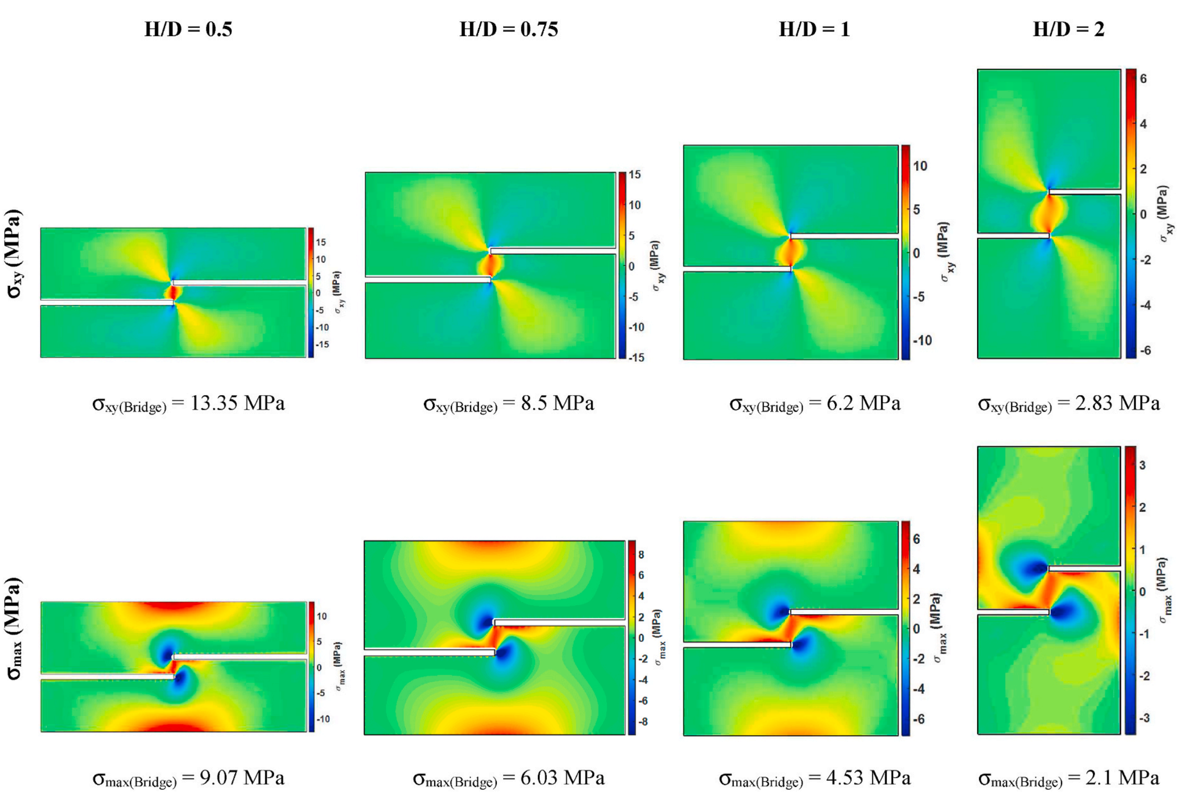

Fig. 10. The effect of H/D ratio on σ_{xy} and σ_{max} for C/H = 0.15, a/D = 0.5 and K = 0.0, $\sigma_V = -1$ MPa.

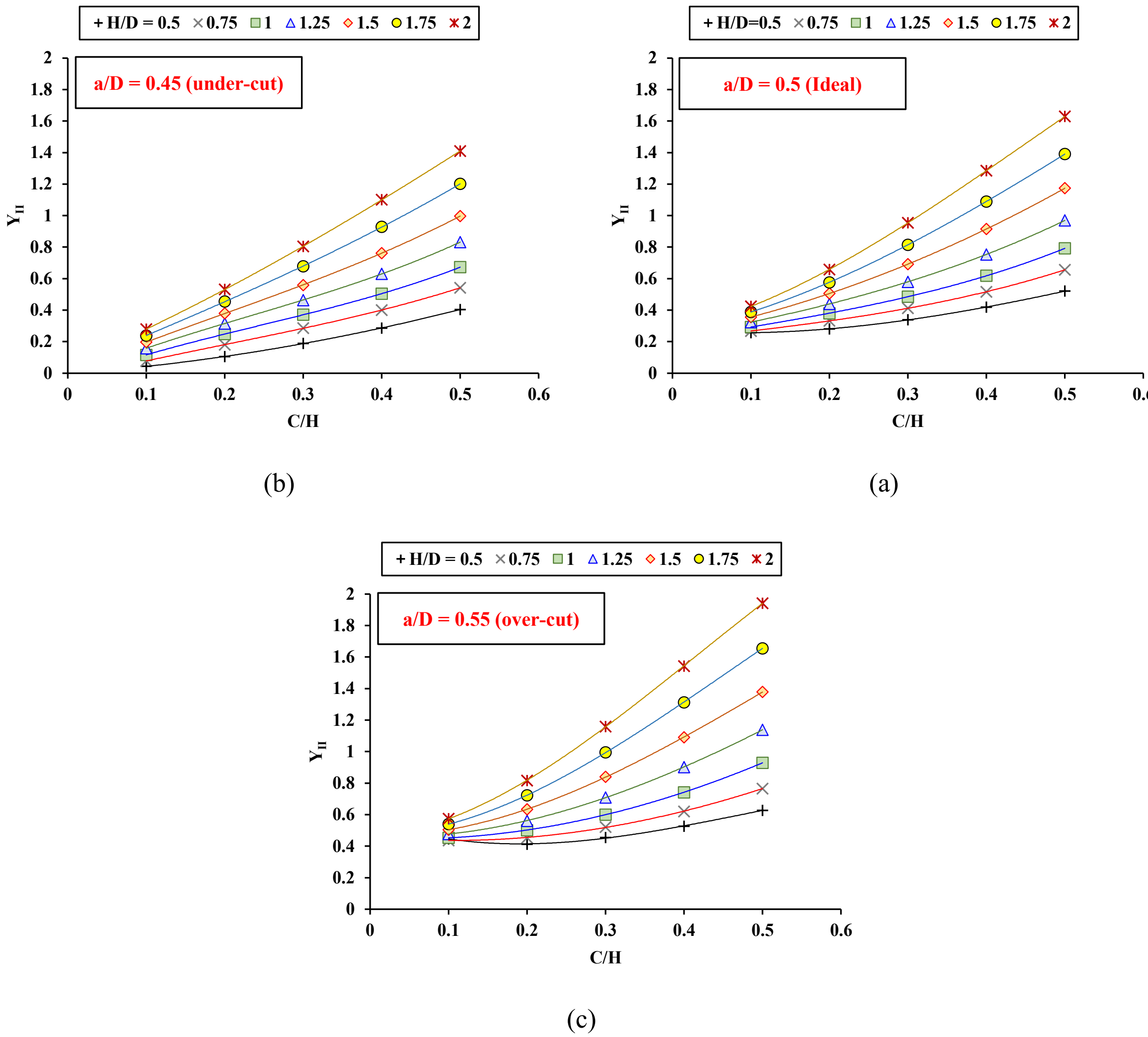

Fig. 11. The effect of H/D, C/H, and a/D ratios on Y_{II} in the SCC sample, with (a) a/D = 0.45, (b) a/D = 0.5, and (c) a/D = 0.55.

using Equation (2):

$$K_{II} = Y_{II}\tau\sqrt{\pi a} = Y_{II}\frac{P}{D\,C}\sqrt{\pi a} \tag{2}$$

where Y_{II} is the dimensionless stress intensity factor, which depends on the geometry of the sample, τ is the shear stress along the bridge between notch tips, and P is the applied load. K_{II} was calculated numerically using Equation (1) and the dimensionless stress intensity factor Y_{II} was obtained using Equation (3):

$$Y_{II} = \frac{K_{II} D\,C}{P\,\sqrt{\pi a}} \tag{3}$$

Using these equations, the effect of the a/D ratio on Y_{II} for H/D = 2 and 1 and different values of the C/H ratio is shown in Fig. 9. This figure shows that Y_{II} increases with increasing the a/D ratio. Moreover, for H/D = 2, Y_{II} is greater than that for H/D = 1 given the same C/H.

Regarding the effect of lateral pressure on the K_{II} and Y_{II}, the results indicated that K_{II} and Y_{II} are independent of lateral pressure. This is because the mode II stress intensity factor is mainly a function of the shear stress along the bridge between notch tips (τ in Equation (2)). As discussed in the previous section, the lateral pressure mainly affects the σ_{max}, and does not affect the σ_{xy}. Note that Fig. 6-c shows the K_{II} predicted by the DDM model of the current study and the FEM model of Yao et al. (2021) as a function of vertical and lateral stresses. This figure shows that the K_{II} is not affected by increasing the lateral pressure from 0 to 25 MPa, and it is mainly affected by vertical stress. As will be shown later in section 4.5, lateral pressure affects the fracture load and the fracture toughness at the moment of fracture.

4.4. *The effect of sample shape (H/D ratio) on stress fields*

For some special considerations, it may be necessary to prepare SCC samples with shapes that are different from the two geometries shown in section 4.1 (H/D = 2 and 1). Therefore, the effect of sample shape was numerically investigated by changing the H/D ratio from 0.5 to 2. The effect of the H/D ratio on σ_{xy} and σ_{max} for C/H = 0.15, a/D = 0.5, and K = 0.0 is shown in Fig. 10. It can be observed that by increasing the H/D ratio from 0.5 to 2, distribution of σ_{xy} is not affected, but the magnitude of this stress at the center of the bridge between notches tips ($\sigma_{xy(Bridge)}$) decreases by about 79%. Shear fracture in the SCC sample grows from tips of two notches and the K_{II} is mainly a function of the shear stress along the bridge between notch tips (τ in Equation (2)). If τ_s is the shear strength of the material and is a material constant, then, a decrease of $\sigma_{xy\,(Bridge)}$ by an increase in H/D ratio indicates an increase in the critical load at the moment of fracture, P_{cr}. Therefore, it can be said that the force required to cause the failure of the SCC sample is directly proportional to the H/D ratio.

With an increase of the H/D ratio, the concentration of the σ_{max} at the upper and lower boundaries of the sample is significantly reduced. For H/D = 2, the effect of the σ_{max} at the upper and lower boundaries of the

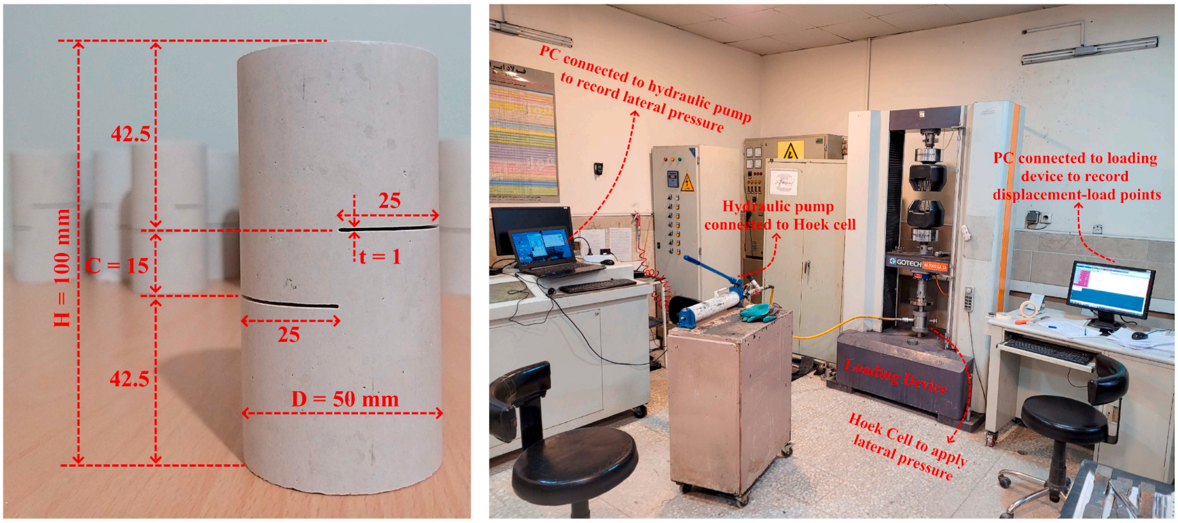

(a) (b)

Fig. 12. (a) Geometry and dimensions of an SCC sample of mudstone used in this paper, (b) loading device and system to apply lateral pressure.

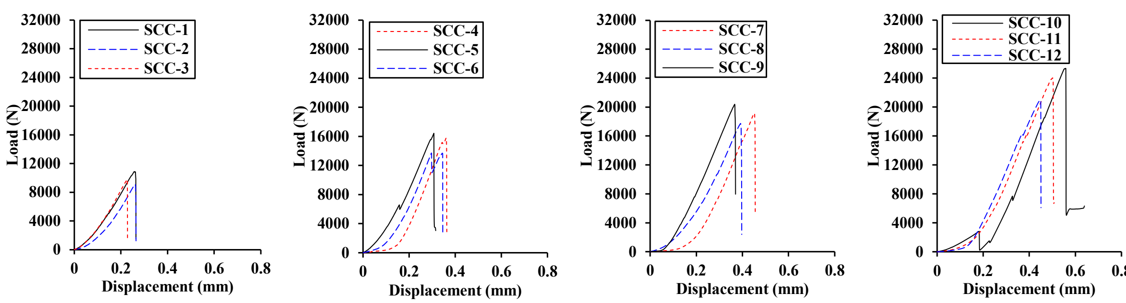

(a) (b) (c) (d)

Fig. 13. The effect of lateral stress on displacement-load curves, (a) $\sigma_H = 0.0$, (b) $\sigma_H = 0.5$, (c) $\sigma_H = 2.0$, and (d) $\sigma_H = 4.0$ MPa.

sample vanishes. As shown in Fig. 10 σ_{max} effect is more pronounced on the sample right and left boundaries near the two notches. In addition, it can be noted that the magnitude of the σ_{max} at the center of the bridge between notch tips ($\sigma_{max(Bridge)}$) decreases by about 77% when the D/H ratio increases from 0.5 to 2.

4.5. *The effect of sample shape (H/D ratio) on the stress intensity factor*

The stress intensity factor K_{II} was calculated using Equation (1) for H/D ratio from 0.5 to 2, C/H from 0.1 to 0.5, and a/D = 0.45, 0.5, and 0.55. Then, Y_{II} was calculated using Equation (3) and the results are shown in Fig. 11. The curves presented in Fig. 11 are considered the most comprehensive in this study as they incorporate the effects of all geometric ratios into account, where they can be used to calculate K_{II} for almost all configurations of SCC samples. It can be observed from the figure that Y_{II} is directly proportional to changes in the H/D, C/H, and a/D ratios.

4.6. *The effect of lateral pressure on the fracture toughness and fracture path in the lab*

To investigate the effect of lateral pressure on the mode II fracture toughness (K_{IIC}), 12 SCC samples of mudstone rock with H/D = 2, C/H = 0.15, and a/D = 0.5 were prepared. Geometry and dimensions are shown in Fig. 12-a. The geometry of H/D = 2 was chosen because as mentioned in section 4.2, the SCC specimen with H/D = 2 is more affected by lateral pressure, where the $\sigma_{max(Bridge)}$ is minimum for H/D = 2 and this promotes the growth of shear fracture along the bridge between notch tips. The loading device and the system used in this study to apply lateral pressure are shown in Fig. 12-b. The SCC sample was laterally stressed by using Hoek cell. The lateral pressure was applied gradually at first by the hydraulic pump, and the pressure was monitored by the PC connected to the hydraulic pump until the desired pressure was reached. Then the SCC sample was vertically loaded by using a loading device until fracture. Twelve SCC samples were tested under lateral stresses of $\sigma_H = 0.0$, 0.5, 2, and 4 MPa, and each test was repeated 3 times to ensure the results. The effect of lateral stress on load-displacement curves is shown in Fig. 13. This figure shows that by increasing σ_H from 0.0 to 4 MPa, the fracture load and the area under load-displacement curves increase. An increase in the fracture load indicates an increase in the mode II fracture toughness (K_{IIC}), while an increase in the area under load-displacement curves indicates an increase in the strain energy stored in the rock sample until fracture. The K_{IIC} was computed using the following equation:

$$K_{IIC} = Y_{II} \frac{P_{cr}}{D\,C} \sqrt{\pi a} \tag{4}$$

where P_{cr} is the fracture load, which corresponds to the peak of the load-displacement curve, D = 50 mm, C = 15 mm, a = 25 mm, and $Y_{II} = 0.69$.

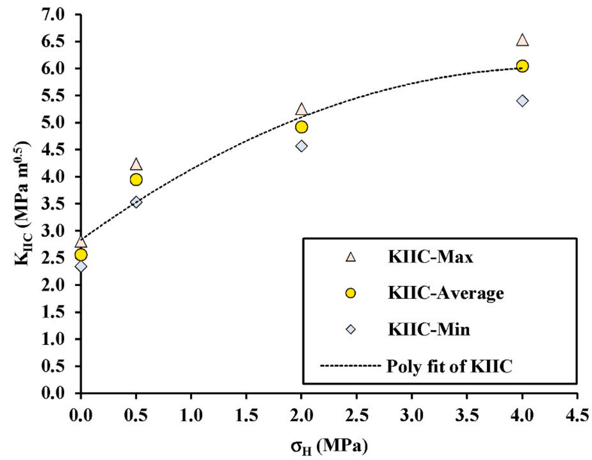

(a)

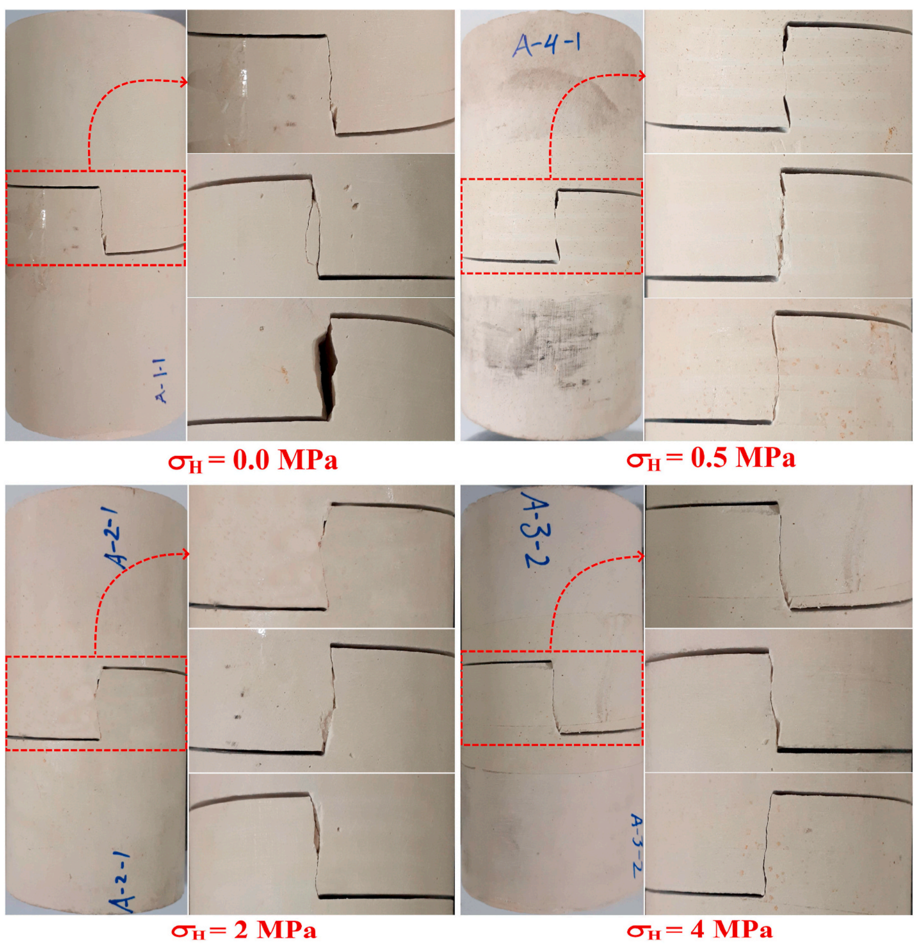

(b)

Fig. 14. (a) Mode II fracture toughness K_{IIC} as a function of lateral stress, $\sigma_{H,}$ (b) Shear fractures in SCC samples after test under different values of lateral stress (0.0–4 MPa).

Y_{II} was obtained from Fig. 9-a for C/H = 0.15 and a/D = 0.5. K_{IIC} as a function of σ_H is shown in Fig. 14-a. This figure shows that the mode II fracture toughness of the shear crack in the SCC sample is directly proportional to the lateral stress. By increasing σ_H from 0.0 (uniaxial case) to 0.5, 2, and 4, the average value of K_{IIC} increases by about 1.54, 1.92, and 2.36 orders of magnitude. This result is consistent with that of Yao et al. (2020) who indicated a rise in fracture toughness with the confining pressure.

Shear fractures in the 12 SCC samples after the test are shown in Fig. 14-b. This figure shows that under a uniaxial compressive stress state ($\sigma_H = 0.0$ MPa), the shear fracture can bifurcate into two fractures. This point was observed in two SCC samples under the uniaxial case. Under the effect of lateral stress, the bifurcation case is not observed in Fig. 14-b, but under σ_H = 0.5 and 2 MPa, some fragments spalled off along the fracture path, and they are highlighted by blue in Fig. 14-b. Under σ_H = 4 MPa, some fragments of the specimen spalled off only in one SCC sample.

5. Conclusion

This study utilized both numerical and experimental methods to investigate shear fractures in SCC samples, with a focus on analyzing the effects of sample configuration and lateral pressure. A numerical TDCPC based on the DDM was extended in this work to model the SCC method, allowing for the examination of the effect of notch length (a/D ratio), sample shape (H/D ratio), and lateral stress (σ_H and K ratio) on shear and maximum principal stress, and stress intensity factor.

The study examined three values of the a/D ratio including 0.45 (under-cut), 0.5 (ideal case), and 0.55 (over-cut). Findings indicated that the case of $a/D < 0.5$ is not optimal as the resulting stress σ_{xy} does not form a continuous bridge between notch tips. However, for $a/D = 0.5$ and 0.55, the resulting fracture should be evaluated to determine whether this fracture is caused by σ_{xy} or σ_{max}.

The study found that increasing the H/D ratio from 0.5 to 2 did not affect the distribution of σ_{xy}, but resulted in a reduction of the stress magnitude along the bridge between the notch tips. Additionally, increasing the H/D ratio reduced significantly the concentration of σ_{max} at the two upper and lower surfaces of the SCC sample. Most importantly, for $H/D = 2$, the effect of σ_{max} at the two upper and lower surfaces of the sample vanishes, while its effect appears on the sample right and left boundaries against the two notches.

The study found that lateral pressure primarily impcated σ_{max}, while leaving the magnitude and distribution of σ_{xy} unaffected. Consequently, the lateral stress did not have an impact on the stress intensity factor K_{II} and its dimensionless form Y_{II}. Thus, the SCC sample with $H/D = 2$ is recommended to be used because a significant decrease in $\sigma_{max(Bridge)}$ is achieved by increasing the lateral stress. This lateral stress inhibits the growth of tensile cracks caused by $\sigma_{max} > 0$ and promotes the growth of shear cracks caused by σ_{xy}. Additionally, it was observed that the fracture toughness K_{IIC} increased in direct proportion to the lateral stress.

Author contribution statement

Mahmoud Alneasan: Methodology, Software, Validation, Formal analysis, Investigation, Writing – original draft, Visualization.; Abdel Kareem Alzo'ubi: Conceptualization, Resources, Investigation, Data curation, Writing – review & editing, Visualization, Supervision, Project administration, Funding acquisition.; Nader Okasha: Writing – review & editing.

Declaration of competing interest

The authors declare that they have no known competing financial interests or personal relationships that could have appeared to influence the work reported in this paper.

Data availability

Data will be made available on request.

Acknowledgment

We would like to thank the ORSP at Abu Dhabi University for funding this project (19300604). We also would like to extend our thanks to Azmoneh Foulad Consulting Engineers[1] for permission to use facilities in his company's rock mechanics lab under the supervision of Eng. Mohsen Aghababaei[2] and Eng. Behzad Nateghpour.[3]

[1] https://en.azmouneh.com/.
[2] . m.aghababaei@mi.iut.ac.ir
[3] . b.nateghpour@mi.iut.ac.ir

References

Aliha, M., Ayatollahi, M., 2010. Geometry effects on fracture behaviour of polymethyl methacrylate. Materials Science and Engineering: A 527, 526–530.
Alneasan, M., Alzo'ubi, A.K., Behnia, M., Mughieda, O., 2022a. Experimental observations on the effect of thermal treatment on the crack speed and mode I and II fracture toughness in brittle and ductile rocks. Theor. Appl. Fract. Mech., 103525
Alneasan, M., Behnia, M., 2022a. Analytical and experimental investigation on the effect of loading rate on the fracture toughness and fracture envelope in brittle rocks. Theor. Appl. Fract. Mech., 103300
Alneasan, M., Behnia, M., 2022b. Analytical model for the activation of off-axis secondary faulting between two dissimilar rock layers. J. Struct. Geol., 104552
Alneasan, M., Behnia, M., Alzo'ubi, A.K., 2022b. Experimental observations on the effect of strain rate on rock tensile fracturing. Int. J. Rock Mech. Min. 160, 105256.
Alneasan, M., Behnia, M., Bagherpour, R., 2020. The effect of Poisson's ratio on the creation of tensile branches around dynamic faults. J. Struct. Geol. 131, 103950.
Alzo'ubi, A., 2016. Modeling Yield Propagation of Jointed Synthetic Rock. In: ISRM International Symposium-EUROCK 2016. OnePetro.
Alzo'ubi, A., 2014. Numerical Simulation of Mechanical Movement of Layered Rock Slopes. In: ISRM International Symposium-8th Asian Rock Mechanics Symposium. OnePetro.
Atkinson, B.K., 1987. Introduction to fracture mechanics and its geophysical applications. Fracture mechanics of rock 1–26.
Ayatollahi, M., Aliha, M., Hassani, M., 2006. Mixed mode brittle fracture in PMMA—an experimental study using SCB specimens. Materials Science and Engineering: A 417, 348–356.
Backers, T., Stephansson, O., 2012. ISRM suggested method for the determination of mode II fracture toughness. In: The ISRM Suggested Methods for Rock Characterization, Testing and Monitoring: 2007-2014. Springer, pp. 45–56.
Bahrami, B., Ghouli, S., Nejati, M., Ayatollahi, M.R., Driesner, T., 2022. Size effect in true mode II fracturing of rocks: theory and experiment. Eur. J. Mech. Solid. 94, 104593.
Crouch, S.L., Starfield, A.M., Rizzo, F., 1983. Boundary element methods in solid mechanics. J. Appl. Mech.90, 704-705.
Fowell, R., Hudson, J., Xu, C., Zhao, X., 1995. Suggested method for determining mode I fracture toughness using cracked chevron notched Brazilian disc (CCNBD) specimens. In: International Journal of Rock Mechanics and Mining Sciences and Geomechanics Abstracts, p. 322A.
Franklin, J., Zongqi, S., Atkinson, B., Meredith, P., Rummel, F., Mueller, W., Nishimatsu, Y., Takahahsi, H., Costin, L., Ingraffea, A., 1988. Suggested methods for determining the fracture toughness of rock. International Journal of Rock Mechanics and Mining & Geomechanics Abstracts 25.
Guo, L., Xiang, J., Latham, J.-P., Izzuddin, B., 2020. A generic computational model for three-dimensional fracture and fragmentation problems of quasi-brittle materials. Eur. J. Mech. Solid. 84, 104069.
Horii, H., Nemat-Nasser, S., 1986. Brittle failure in compression: splitting faulting and brittle-ductile transition. Phil. Trans. Roy. Soc. Lond. Math. Phys. Sci. 319, 337–374.
Horii, H., Nemat-Nasser, S., 1985. Compression-induced microcrack growth in brittle solids: axial splitting and shear failure. J. Geophys. Res. Solid. 90, 3105–3125.
Jung, Y., Park, E., Kim, H., 2016. Determination of mode II toughness of granite by using SCC test. In: ISRM International Symposium-EUROCK 2016. OnePetro.
Kim, B.-H., Larson, M.K., 2021. Laboratory investigation of the anisotropic confinement-dependent brittle-ductile transition of a Utah coal. Int. J. Min. Sci. Technol. 31, 51–57.
Kuruppu, M.D., Obara, Y., Ayatollahi, M.R., Chong, K., Funatsu, T., 2014. ISRM-suggested method for determining the mode I static fracture toughness using semi-circular bend specimen. Rock Mech. Rock Eng. 47, 267–274.
Li, D., Xiao, P., Han, Z., Zhu, Q., 2020. Mechanical and failure properties of rocks with a cavity under coupled static and dynamic loads. Eng. Fract. Mech. 225, 106195.
Li, D., Zhang, C., Zhu, Q., Ma, J., Gao, F., 2022a. Deformation and fracture behavior of granite by the short core in compression method with 3D digital image correlation. Fatig. Fract. Eng. Mater. Struct. 45, 425–440.
Li, X., Xu, Y., Zhan, Z., Yao, W., Xia, K., 2022b. Influence of thermal treatment on dynamic mode II fracture properties of rocks using the short core in compression (SCC) method. Theor. Appl. Fract. Mech. 119, 103383.
Mousavi, S., Aliha, M., Imani, D., 2020. On the use of edge cracked short bend beam specimen for PMMA fracture toughness testing under mixed-mode I/II. Polym. Test. 81, 106199.
Nemat-Nasser, S., Horii, H., 1982. Compression-induced nonplanar crack extension with application to splitting, exfoliation, and rockburst. J. Geophys. Res. Solid. 87, 6805–6821.
Rao, Q., Sun, Z., Stephansson, O., Li, C., Stillborg, B., 2003. Shear fracture (Mode II) of brittle rock. Int. J. Rock Mech. Min. 40, 355–375.
Shou, K., Crouch, S.L., 1995. A higher order displacement discontinuity method for analysis of crack problems. Int. j. rock mech. min. sci. geomech. abstr. Elsevier 49–55.
Szwedzicki, T., 2003. Quality assurance in mine ground control management. Int. J. Rock Mech. Min. 40, 565–572.
Wang, Q., Feng, F., Ni, M.-q., Gou, X., 2011. Measurement of mode I and mode II rock dynamic fracture toughness with cracked straight through flattened Brazilian disc impacted by split Hopkinson pressure bar. Eng. Fract. Mech. 78, 2455–2469.
Watkins, J., Liu, K., 1985. A finite element study of the short beam test specimen under mode II loading. Int. J. Cem. Compos. Lightweight Concr. 7, 39–47.
Xu, Y., Yao, W., Zhao, G., Xia, K., 2020. Evaluation of the short core in compression (SCC) method for measuring mode II fracture toughness of rocks. Eng. Fract. Mech. 224, 106747.

Yao, W., Wang, J., Wu, B., Xu, Y., Xia, K., 2022. Dynamic mode II fracture toughness of rocks subjected to various in situ stress conditions. Rock Mech. Rock Eng. 1–18.

Yao, W., Xu, Y., Wang, C., Xia, K., Hokka, M., 2021. Dynamic Mode II fracture behavior of rocks under hydrostatic pressure using the short core in compression (SCC) method. Int. J. Min. Sci. Technol. 31, 927–937.

Yao, W., Xu, Y., Xia, K., Wang, S., 2020. Dynamic mode II fracture toughness of rocks subjected to confining pressure. Rock Mech. Rock Eng. 53, 569–586.

Zhang, C., Li, D., Ma, J., Zhu, Q., Luo, P., Chen, Y., Han, M., 2023. Dynamic shear fracture behavior of rocks: insights from three-dimensional digital image correlation technique. Eng. Fract. Mech. 277, 109010.

Zhang, C., Li, D., Wang, C., Ma, J., Zhou, A., Xiao, P., 2022a. Effect of confining pressure on shear fracture behavior and surface morphology of granite by the short core in compression test. Theor. Appl. Fract. Mech. 121, 103506.

Zhang, K., Hamada, S., Shindome, K., Yokoi, T., Noguchi, H., 2022b. Early crack initiation mode during tensile fracture process in a punch-processed precipitation-hardened steel plates and evaluation method to treat the crack as an equivalent pre-crack. Materials Science and Engineering: A 850, 143534.